Evidence for premature aging due to oxidative stress in iPSCs from Cockayne syndrome

Luciana Nogueira de Sousa Andrade[1,2,3], Jason L. Nathanson[2], Gene W. Yeo[2], Carlos Frederico Martins Menck[3] and Alysson Renato Muotri[1,2,*]

[1]School of Medicine, Department of Pediatrics/Rady Children's Hospital San Diego and [2]Department of Cellular & Molecular Medicine, University of California San Diego, Stem Cell Program, 2880 Torrey Pines Scenic Road - Sanford Consortium, La Jolla, CA 92093, MC 0695, USA and [3]Department of Microbiology, DNA Repair Laboratory, Biomedical Institute, University of São Paulo, 1374 Av. Prof. Lineu Prestes, São Paulo, SP 05508-000, Brazil

Cockayne syndrome (CS) is a human premature aging disorder associated with neurological and developmental abnormalities, caused by mutations mainly in the CS group B gene (*ERCC6*). At the molecular level, CS is characterized by a deficiency in the transcription-couple DNA repair pathway. To understand the role of this molecular pathway in a pluripotent cell and the impact of CSB mutation during human cellular development, we generated induced pluripotent stem cells (iPSCs) from CSB skin fibroblasts (CSB-iPSC). Here, we showed that the lack of functional CSB does not represent a barrier to genetic reprogramming. However, iPSCs derived from CSB patient's fibroblasts exhibited elevated cell death rate and higher reactive oxygen species (ROS) production. Moreover, these cellular phenotypes were accompanied by an up-regulation of *TXNIP* and *TP53* transcriptional expression. Our findings suggest that CSB modulates cell viability in pluripotent stem cells, regulating the expression of *TP53* and *TXNIP* and ROS production.

INTRODUCTION

Cockayne Syndrome (CS) is a rare autosomal recessive human disorder characterized by hypersensitivity to sunlight and neurodegeneration along with symptoms of premature aging, retinal degeneration, cachectic dwarfism, cataracts and loss of subcutaneous fat (1). A recent study showed that two-third of CS cases are caused by mutations in the excision-repair cross complementing group 6 (*ERCC6*) gene, while remaining cases are caused by mutations in the *ERCC8* gene, even though the clinical symptoms are indistinguishable (2). The *ERCC6* gene codifies a protein named Cockayne syndrome group B protein (CSB), a member of the SWI2/SNF2 family of ATP-dependent chromatin remodelers (3,4). In addition, CSB is involved in many biological processes including DNA repair and transcription (5,6), regulation of specific genes after oxidative stress (7) and regulation of hypoxia response (8). However, most of the studies involving CSB are related to its role in DNA repair. CSB plays an important role in the Nucleotide Excision Repair (NER) pathway. It is

assumed that the blockage of RNA polymerase II triggers the recruitment of CSB to the DNA damage site, which is responsible for the subsequent accommodation of NER proteins, chromatin remodelers and CSA-E3-ubiquitin ligase complex, activating the transcription-coupled repair (TCR-NER) sub-pathway. TCR is responsible for the removal of lesions in the transcribed strand (reviewed in 9). Besides NER, CSB is also involved in the removal of certain types of oxidative damage in nuclei and mitochondria (10,11), suggesting an interaction between CSB and the base excision repair—the pathway involved in the removal and repair of oxidative DNA damage.

Interestingly, it has been suggested that altered transcription, defective DNA repair pathways and accumulation of oxidative damage are involved in normal cellular aging and progeroid syndromes (12,13). The role of CSB in these processes might explain some clinical aspects of CS. Recently, two independent groups (14,15) generated patient-derived induced pluripotent stem cells (iPSCs) for Hutchinson-Gilford Progeria Syndrome (HGPS), providing a novel tool for

*To whom correspondence should be addressed at: Department of Pediatrics/Rady Children's Hospital San Diego, Department of Cellular & Molecular Medicine, University of California San Diego, School of Medicine, Stem Cell Program, 2880 Torrey Pines Scenic Road, Sanford Consortium, Room 3005, La Jolla CA, 92093-0695, USA. Tel: +1 8585349320; Fax: +1 8582461579; Email: muotri@ucsd.edu

understanding the molecular basis of aging. These works suggest that the accumulation of progerin in mesenchymal stem cells (MSC) and vascular smooth muscle cells, both derived from HGPS-iPSCs, leads to an increase in DNA damage, nuclear abnormalities and enhanced cell sensitivity to stressful conditions, such as hypoxia. Since the MSC niche has low oxygen levels, such an environment could cause depletion in MSCs, compromising tissue repopulation and accelerating the aging process.

Here, we investigated the contribution of CSB during cellular reprogramming and maintenance of the pluripotent state. By converting skin fibroblasts from a CSB patient with mutation in the *ERCC6* gene to iPSCs, we showed that CSB is not essential for reprogramming but has critical roles in maintenance and viability of pluripotent cells. CSB-iPSCs are characterized by an up-regulation of *TP53* and *TXNIP* genes and increased reactive oxygen species (ROS) production. Such phenotypes are correlated to a massive cell death that might be related to the premature aging observed in CS patients.

RESULTS

Generation and characterization of iPSC clones from a CSB patient

Human fibroblasts GM10903 (Coriell Cell Repository), carrying the Arg735Ter (R735X) mutation in the *ERCC6* gene (16), were transduced with individual retroviral vectors containing the four human versions of the Yamanaka factors (*c-Myc, Klf4, Oct3/4 and Sox2*) (17). After 2 weeks, we observed individual tightly packed colonies, similar to human embryonic stem cells (hESC), with high nuclear to cytoplasm ratio (Fig. 1A). Immunostaining of individual clones with pluripotent markers revealed expression of Nanog, Lin28, Oct4, Sox2 and SSEA-4 (Fig. 1B–D). Quantitative reverse transcription–polymerase chain reaction (RT-PCR) analysis showed that independent CSB-iPSC clones expressed pluripotent-specific genes. All clones showed increased expression of Nanog, Oct4 and Sox2 compared with CSB fibroblasts (Fig. 1E). To confirm reprogramming at the molecular level, transcriptional analysis using human genome Affimetrix Gene Chip arrays were performed using RNA isolated from three CSB-iPSC clones, two control [wild-type (WT)] iPSCs and respective donor fibroblasts. Hierarchical clustering of all genes revealed that all iPSC clones clustered together and showed a similar global gene expression to two hESC lines, H1 and HUES6 (Fig. 1F). To exclude any possibility of chromosomal abnormalities due to the lack of TCR-NER, we examined the karyotype of individual CSB-iPSC and donor fibroblasts. CSB-iPSC karyotype remained normal and identical to the donor fibroblasts (Fig. 1G). We then tested the ability of CSB-iPSC to form embryoid bodies (EBs) *in vitro*. After 2 weeks in suspension without FGF2, EBs were harvested and quantitative RT–PCR was performed. Evidence for cells expressing markers of the three germ layers were found (Fig. 1H and I). Teratomas were obtained from WT and CSB-iPSCs as another evidence of pluripotency. However, we noticed a teratoma growth failure in animals injected with the same number of CSB-iPSCs when compared with WT-iPSCs, preventing further histological analyses.

A striking visual difference in teratomas derived from CSB-iPSCs is the reduction in blood vessels (Fig. 1J).

Increased iPSC death in the absence of CSB

The growth failure of teratomas derived from CSB-iPSCs may suggest an increased amount of cell death. In fact, we also noticed a slower growth rate during routine maintenance of CSB-iPSCs compared with normal (WT) iPSC clones: the split ratio of CSB-iPSCs was much lower compared with normal iPSCs (1:2 and 1:4–1:5, respectively). To evaluate whether the lack of a functional CSB protein could compromise cell survival in pluripotent stem cells, we quantified the sub-G1 population, representing dead cells with fragmented DNA, in three independent CSB-iPSC clones by flow cytometry. The percentage of dead cells was ~3-fold greater in CSB-iPSC clones compared with control iPSCs. Interestingly, we did not detect any difference in donor fibroblast cells when comparing CS with WT (Fig. 2A and B). To confirm that the elevated cell death ratio was due to the lack of functional CSB, human H9 embryonic stem cells were transfected with either a control shRNA plasmid (shRNA-scrambled) or plasmid expressing shRNA against CSB (shRNA-CSB). After 48 h, cells were collected and analyzed by fluorescence-activated cell sorting. We observed a significant increase in the sub-G1 population in H9 cells expressing shRNA-CSB in comparison to control, corroborating our finding (Fig. 2C). Based on the fact that p53 is a master regulator of cell survival and death in response to DNA damage (reviewed in 18), we next examined the *TP53* gene expression levels in those clones by quantitative RT–PCR. We found that *TP53* is ~3-fold up-regulated in CSB-iPSC clones compared with clones obtained from control iPSCs (Fig. 2D). Moreover, *p21* (*WAF1/CIP1*) levels, a downstream target of p53, and other relevant CDKIs (cyclin-dependent kinase inhibitors) remained unchanged in all clones as revealed in our microarray analysis (Fig. 2E).

Gene expression analysis in CSB-iPSCs revealed defects in ROS response

t-Test statistical comparisons between samples yielded 350 probes that were up-regulated and 238 probes were down-regulated in CSB-iPSC relative to embryonic stem cells H1 (individual comparison *P*-values < 0.01). These differentially regulated genes were classified using DAVID gene ontology analysis. Although DNA repair genes were not an over-represented group by gene ontology classification, the microarray data indicated a 2-fold decrease in *BRCA2* levels in CSB-iPSCs, a gene known to inhibit p53's transcriptional activity in cancer cells (data not shown) (19). The down-regulation of *BRCA2* is consistent with a potential role in the up-regulation of p53 in CSB-iPSCs. *BRCA1* expression levels did not change. Of the genes significantly mis-regulated in the CSB-iPSCs relative to controls, we observed an up-regulation in three members of the α-arrestin family of proteins (ARRDC3, ARRDC4 and TXNIP) in all CSB-iPSC clones. In fact, *TXNIP* (thioredoxin interacting protein) was one of the most up-regulated genes that encodes an endogenous inhibitor of thioredoxin (TRX) which, together with
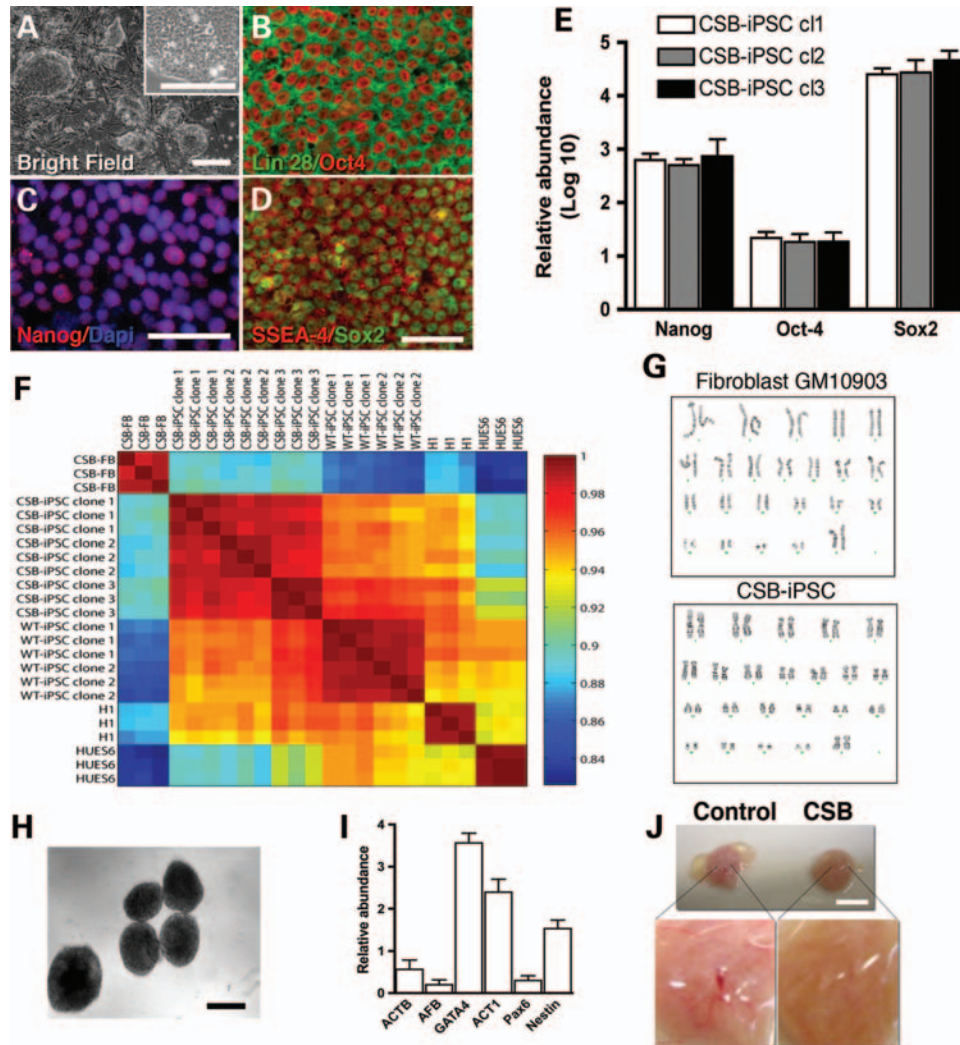
Figure 1. Generation and characterization of CSB-iPSCs. (**A**) Phase contrast image of emerging colonies of CSB-iPSC cells on MEFs 10 days after viral infection. Inset: high magnification of a CSB-iPSC colony displaying cells with a high nucleus/cytoplasm ratio. Bar = 50 μm. (**B–D**) Immunofluorescence staining of pluripotency-associated markers Lin28, Oct3/4, Nanog, SSEA-4 and Sox2 in CSB-iPSC cells. Bar = 50 μm. (**E**) *Nanog, Oct3/4 and Sox2* expression levels in three distinct CSB-iPSC-derived clones by qPCR ($n = 3$ for each clone). The data are presented as means ± SD. (**F**) Correlation distances between samples were calculated using vectors of RMA intensity values for all genes on the microarray (MATLAB 7.7, corrcoef). All iPSC clones correlate well with two hESC lines, and less well to donor fibroblasts, indicating reprogrammed iPSCs have similar transcription profiles to hESCs. (**G**) Absence of gross chromosomal abnormalities on the karyotype of CSB-iPSCs. (**H**) Differentiation of CSB-iPSCs into embryoid bodies (EB) *in vitro*. Bar = 50 μm. (**I**) RT–PCR of relative quantification of endo (*AFP* and *GATA* 4), meso (*ACT1* and *ACTB*) and ectodermal (*Pax 6* and *Nestin*) specific genes. The *y*-axis represents fold change relative to CSB-iPSC expression levels. The data are presented as means ± SD ($n = 3$ for each clone). (**J**) Teratoma obtained from Control and CSB-iPSCs. The detail reveals the lack of blood vessels in CSB-iPSC derived teratomas. Bar = 100 μm.

glutathione, constitute the cellular thiol reduction systems that act as scavengers of ROS (20,21) (Fig. 2F).

We also analysed the global expression of microRNAs. MicroRNAs were cloned and sequenced for two of the CSB-iPSC clones, and compared to data from five WT-iPSC clones and two hESC lines. Small RNA reads were mapped to the human genome, and aligned with coordinates of known microRNAs (22–25). Mature microRNAs are the processed products of precursor and primary RNA. These processes are heterogenous, and can result in multiple microRNA species from the same precursors, so-called isomiRs (26,27). The microRNA seed sequence, generally accepted as important for mRNA target identification, begins at base 2 from the 5′ end of the microRNA. Therefore, isomiRs with different 5′ start sites would be predicted to have different mRNA targets. Our data indicate that numerous isomiRs may be mis-regulated in CSB-iPSCs. Using TargetScan seed predictions (28), we correlated mis-regulated isomiRs and mRNA. Although there did not appear to be a global bias for predicted microRNA-binding sites among up- or down-regulated genes (Supplementary Material, Table S1), many genes did have binding sites consistent with potential down-regulation by microRNA binding. In fact, hsa-mir-106a[1] and hsa-mir-3609[-1] are predicted to target the TXNIP 3′UTR. In addition, the CSB up-regulated genes ARDDC3 and ARDDC4 have predicted sites for the down-regulated micro-RNAs hsa-mir-19b-1[0], hsa-mir-19b-2[0] and hsa-mir-19a[0]. Moreover, inhibition of hsa-mir-19a has been shown
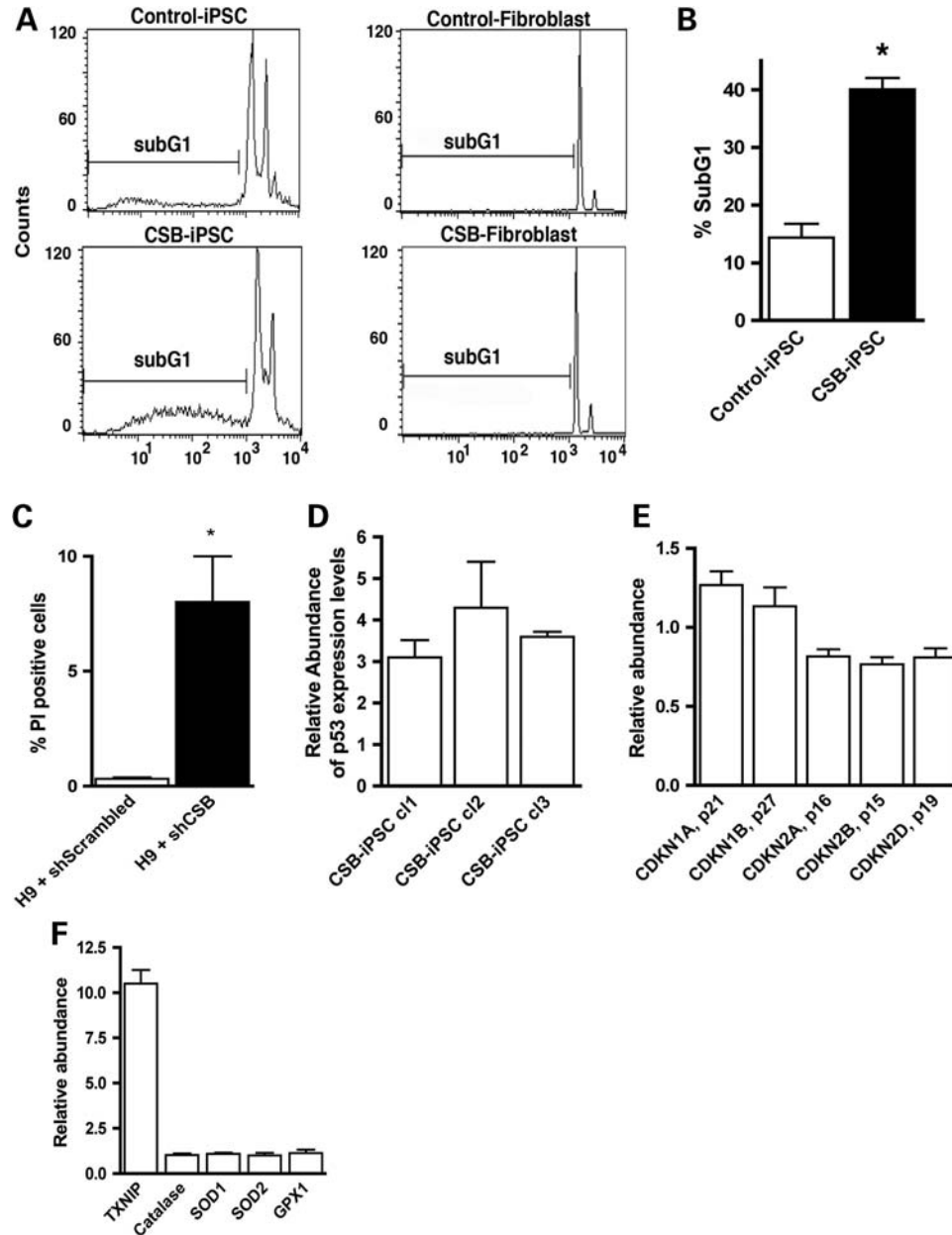
Figure 2. Cell death in CSB-iPSC. (**A** and **B**) Flow cytometry analysis of dead cells (represented by sub-G1 content) in CSB-iPSCs and fibroblasts. Each bar represents the mean $\pm$ SD ($n = 2-7$). Statistical analyses were performed using t-test one-tailed and differences were considered significant for $P < 0.05$ (indicated by asterisk). Flow data from representative samples are shown. In (**C**), cell death analysis of human H9 ES transfected with a control (shRNA-Scrambled) or plasmid expressing shRNA against CSB (shRNA-CSB). Each bar represents the mean $\pm$ SD ($n = 3$) of H9 ES dead cells. The y-axis represents the percentage of propidium iodide (PI) positive cells (dead cells) determined by flow cytometry. Statistical analyses were performed using t-test one-tailed and differences were considered significant for $P < 0.05$ (indicated by asterisk). (**D**) RT–PCR for *TP53* expression in distinct clones of both control and CSB-iPSCs. The y-axis represents fold change relative to *TP53* levels in Control iPSCs. The data are presented as mean ($n = 3$). (**E**) Cell cycle regulators mRNA levels in CSB-iPSCs. The y-axis represents fold change relative to each gene level in control. The data are presented as means $\pm$ SD (triplicate for each clone). (**F**) mRNA level measurements by microarray of cell mediators of oxidative stress in CSB-iPSCs. The y-axis represents fold change relative to each gene level in control. The data are presented as means $\pm$ SD (triplicate for each clone).

to induce apoptosis in esophageal squamous cell carcinoma (29), suggesting a possible role of this hsa-mir-19a in controlling cell death in CSB-iPSCs.

Elevated ROS levels in CSB-iPSC

Based on the fact that CSB also plays an important role in the removal of oxidative lesions and the accumulation of intracellular ROS is associated with increased cell death and aging (30,31), we next investigated the endogenous levels of ROS in CSB-iPSCs. We used a specific fluorigenic marker for ROS, carboxy-H_2DCFDA (carboxy-2′,7′-dichlorodihydrofluorescein diacetate) in live cells, plated at identical cell densities. Compared with control iPSCs, we noticed a 3-fold increase in the number of ROS-positive cells and brighter intensity in
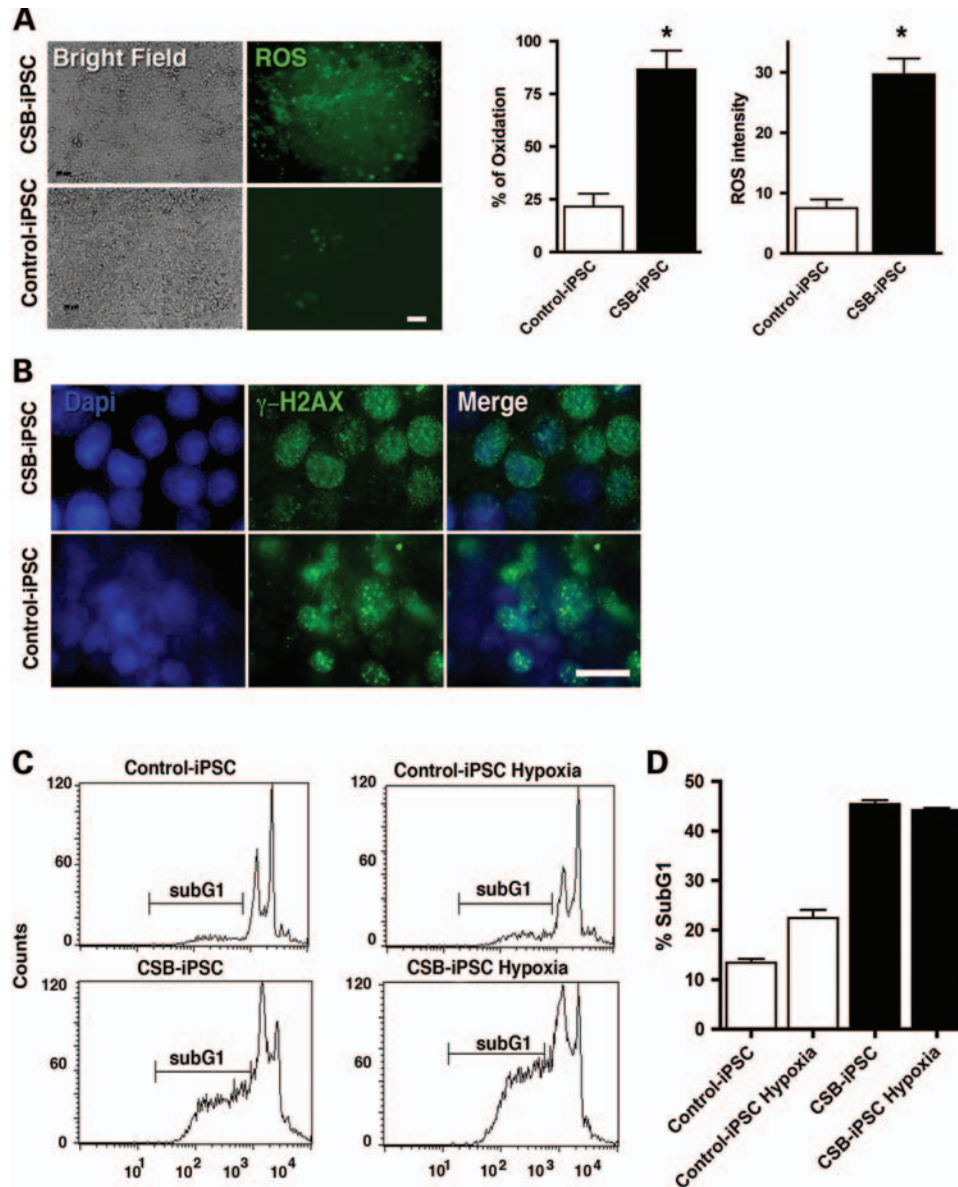
Figure 3. Quantification of the production of ROS in control and CSB-iPSCs. (**A**) Images were taken after incubation with H_2DCFDA in control and CSB-iPSCs plated at the same density (bar = 50 µm). Bar graphs in the right show percentage of cells producing ROS and fluorescence intensity. Mean ± SD ($n = 3$). Statistical analyses were performed using *t*-test one-tailed and differences were considered significant for $P < 0.05$ (indicated by asterisk). (**B**) DDR activation in CSB-iPSCs. Immunofluorescence staining shows the presence of γ-H2AX at similar levels in both CSB and Control iPSCs. Representative images are shown. Bar = 15 µm. (**C** and **D**) Cell death evaluation under hypoxia. Flow cytometry analysis of sub-G1 content in control and CSB-iPSCs cultivated under hypoxia conditions for 24 h. Bar graph shows the percentage of dead cells in normoxia and hypoxia. Representative samples are shown.

CSB-iPSCs (Fig. 3A). These data suggest that the lack of functional CSB in iPSCs induces higher levels of ROS, even in the absence of an exogenous stimulus. To gain insights on molecular pathways that could be involved in this phenomenon, we examined the mRNA levels of genes involved in the cellular response to oxidative stress. Our gene expression analysis showed no significant differences between normal and CSB-iPSCs in catalase, superoxide dismutase and glutathione levels. However, the upregulation of *TXNIP* in CSB-iPSC clones indicates that this molecular pathway could contribute to the higher levels of intracellular ROS as illustrated in Figure 2F.

Activation of DNA damage response (DDR) in CSB-iPSC

A variety of genotoxic stresses lead to certain types of lesions in DNA that activate the DNA damage response (DDR). At the molecular level, DDR is characterized by the phosphorylation of the histone variant H2AX, being responsible for the recruitment of DDR proteins at the site of a lesion. It is known that ROS attack DNA readily, generating a variety of DNA lesions, such as oxidized bases and strand breaks that induce the phosphorylation of H2AX (reviewed in 32). Thus, we measured the activation of DDR in CSB or control iPSCs, using antibodies against γH2AX (the phosphorylated form of H2AX). No

difference was noticed in nuclear distribution of γH2AX and γH2AX-positive cells were present in both genotypes at similar levels (Fig. 3B).

Maintenance of CSB-iPSCs under hypoxic conditions

Adult stem cells may reside in niches with low oxygen tension (hypoxia), which can compromise cell viability in the absence of functional DNA repair proteins, such as CSB (8). Thus, we next evaluated whether hypoxia could affect the viability of CSB-iPSCs. Control and CSB-iPSC clones were cultured in the presence of cobalt chloride (150 μM), a known inducer of hypoxia (33), for 24 h, after which, percent cell death was evaluated by flow cytometry. The induction of hypoxic conditions was confirmed by the expression of HIF1-α, the subunit of the hypoxia inducible factor (HIF) that is constantly degraded under normoxia (34). No differences in cell death were observed in CSB-iPSCs, indicating that CSB does not play a role in hypoxia response in pluripotent cells (Fig. 3C and D).

DISCUSSION

Since its initial discovery by Takahashi and Yamanaka (35), genetic reprogramming has been performed in several cell types, including somatic cells from different animal species (36,37). Recently, some groups have shown the existence of molecular barriers that impair reprogramming of differentiated cells into iPSC, such as senescence (38), the tumor suppressor gene *TP53* (39,40) and the *INK4a/Arf* locus (41,42). In addition, Marión *et al.* (39) and Raya *et al.* (43) observed that DNA damage also prevents the reprogramming of somatic cells. Here, we have generated iPSC from skin fibroblast of a patient with CS, characterized at the molecular level by the lack of functional CSB and the TCR-NER pathway. Our data revealed that CSB fibroblasts could be successfully reprogrammed, showing that is possible to convert DNA repair compromised cells into stem cells.

However, after reprogramming, the growth rate of CSB-iPSC cells was significantly slower than normal iPSC, suggesting that these cells could exhibit cell cycle arrest and/or increased death rate. In fact, flow cytometry analysis showed an elevated cell death rate in CSB-iPSCs without any significant alterations in the cell cycle profile. Due to the size of the CSB cDNA, we were unable to perform gain-of-function experiments. However, the knockdown of CSB in human ES using shRNAs also led to a significant increase in cell death, consistent with our findings. Interestingly, donor CSB fibroblasts showed no alterations in cell death compared with control fibroblasts, indicating that CSB may play a role in pluripotent cell viability. Recently, Fong *et al.* (44) showed that XPC (Xeroderma pigmentosum group C), a component of Genome Global Repair pathway (GGR-NER), altogether with RAD23B and Centrin 2 (CETN2), is essential for somatic cell reprogramming and stem-cell renewal. The authors showed that this heterotrimeric complex promotes Nanog expression and its knockdown in ES cells promotes differentiation followed by rapid apoptosis, as we observed for

CSB-iPSCs. Moreover, we also speculate that the slower growth of teratomas originating from CSB-iPSC might be due to elevated CSB-iPSCs death.

At the molecular level, we did not find significant differences in CDKI levels, corroborating the idea that the elevated CSB-iPSC death rate is not preceded by cell cycle arrest. To determine the molecular pathway affected, we examined the levels of several pro-apoptotic genes and found a significant increase in *TP53* expression in CSB-iPSC clones. The up-regulation in this gene was accompanied by a down-regulation in *BRCA2* levels, a known inhibitor of p53.

We used the fluorigenic marker carboxy-H_2DCFDA to detect the levels of ROS in live iPSCs. We observed that the lack of functional CSB leads to a higher production of ROS in iPSCs, affecting cell viability. At the molecular level, our analysis showed an upregulation of TXNIP mRNA levels in CSB-iPSCs, which might be caused by the down-regulation in hsa-mir-106a and hsa-mir-3609 microRNAs. An increase in TXNIP levels has been correlated with increased levels of intracellular ROS, decreased growth rate and/or cell death and cellular aging (45–47). We hypothesize that the higher levels of ROS in CSB-iPSC are due to the up-regulation in TXNIP mRNA levels, which causes an increase in p53 levels and cell death.

The observation that CSB-iPSCs are under oxidative stress lead us to investigate the activation of the DDR in these cells. We examined DDR activation by the presence of γH2AX. However, the levels of γH2AX in CSB-iPSCs are similar to control, suggesting that damaged cells are being eliminated by prompt activation of cell death, as proposed by Marión *et al.* (39). It was previously shown that under hypoxic conditions, CSB in fibroblasts modulates p53 activity, favoring cell survival and proliferation (48). Curiously, we did not observe an increase in CSB-iPSC death under hypoxia or any difference in the levels of cellular mediators involved in hypoxia response as observed in CSB deficient fibroblasts (4). Our data suggest that CSB plays a role in the hypoxic pathways favoring survival exclusively in differentiated cells.

Here, we show that a defective TCR-NER, due to the lack of functional CSB, does not necessarily represent a cellular barrier for genetic reprogramming. Our results demonstrated that CSB plays a role in the maintenance of cell survival in pluripotent cells, possibly by eliminating cells with an accumulation of oxidative DNA damage. Such a mechanism may be associated with premature aging in CS. Our model suggests that CSB down-regulates TXNIP expression affecting intracellular ROS levels, whereas p53 remains at normal levels (Fig. 4).

MATERIALS AND METHODS

Cell cultures

GM10903 human skin fibroblasts were obtained from Coriell Cell Repositories. The cells were maintained in Dulbecco's modified eagle medium (DMEM) (Life Technologies) containing 15% fetal bovine serum (FBS, Omega). We used the control iPSC (WT-126 clones 1 and 7), as previously described (49).
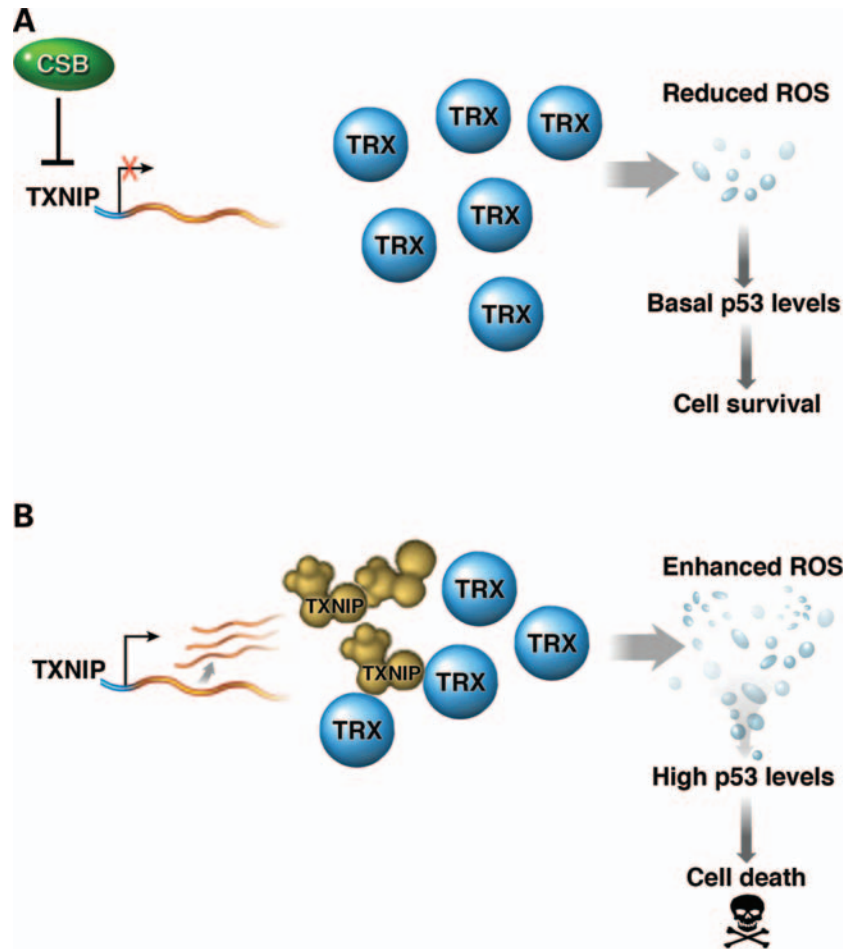
Figure 4. CSB plays a role in pluripotent stem cell survival. According to our model, CSB inhibits *TXNIP* transcription, preventing the blockage of TRX scavenger activity and favoring cell survival (**A**). In contrast, the absence of functional CSB would increase *TXNIP* transcription and its interaction with TRX, leading to an increase in intracellular ROS levels. As a consequence, *TP53* is up-regulated, triggering cell death (**B**).

Retroviral vector production and cellular reprogramming

HEK 293T cells were maintained in DMEM high glucose (Life Technologies) containing 10% FBS. Cells were then co-transfected with pMXs retroviral vectors containing the human cDNA for *c-Myc, Klf4, Oct3/4, Sox2* VSGV and CMVgp (Addgene) with the cationic polymer PEI (Polyethylenimine). After 2 days, the media were collected, filtered and centrifuged at 60 000g for 2 h at 4°C when the virus were resuspended in DMEM high glucose. GM10903 CSB fibroblasts were seeded at 10×10^4 cells/well of a six-well plate and 24 h later the media were replaced by DMEM high glucose containing the viral vectors. After 6 h, the media were switched to DMEM plus 10% FBS. Two days after the transduction, the cells were harvested and re-plated on a 10 cm dish with mouse embryonic fibroblast (MEF, Millipore). The culture media were replaced by hESC media (DMEM/F12 media Glutamax, Gibco), 20% knockout serum replacement, 1% non-essential amino acids, 0.2% β-mercaptoethanol, 30 ng/ml FGF-2 (Life Technologies) the next day. After 24 h, 1 mM valproic acid (Sigma) was added in the media for 5 days. Individual iPSC colonies were plated on matrigel (BD) coated plates after 3 weeks when the media were switched to mTeSR (Stemcell Technologies). Individual colonies of iPSCs were manually passed and maintained on feeder-free condition. Three clones were selected for further characterization.

RNA extraction and RT–PCR

RNA was extracted from CSB-iPSC clones, EBs and GM10903 fibroblasts using Trizol® (Life Technologies). All samples were treated with DNAse (Ambion) to avoid genomic contamination. cDNA was synthesized using the Superscript III First-Strand Synthesis System RT-PCR (Life Technologies) according to the manufacturer's instructions. The cDNA was amplified by real-time PCR using the Perfecta qPCR Fast Mix for pluripotent and differentiated markers (Quanta Biosciences). For *TP53* levels, we used Taq DNA polymerase (Fermentas) and the primers sequences were: F-5′GGGCTCCGGGGACACTTTGC3′ and R-5′ CTGGCT GCCAATCCAGGGAAGC3′. These sequences were designed for p53 RNA sequence NM_00546.4 using Primer Blast tool.

Karyotype analysis

Standard G-Banding chromosome analysis was performed by Cell Line Genetics (Madison, WI, USA) and Molecular Diagnostic Services, Inc. (San Diego, CA, USA).

Microarray analysis

Three Human Gene 1.0 ST (HuGene-1.0-st) microarrays (Affymetrix) were probed with cDNA for each of the cell types [CSB-FB (fibroblasts), CSB-iPSC clones 1, 2 and 3, WT-iPSC clones 1 and 2; H1 and HUES6]. Log2-transformed probe intensity values were calculated using default RMA analysis parameters using Expression Console v1.1 software (Affymetrix) and the HuGene-1.0-st-v1.r4 library file downloaded from Affymetrix. Correlation coefficients between samples were calculated using vectors of RMA intensity values for all genes (MATLAB7.7, corrcoef). Statistical comparisons between CSB-iPSC and H1 were calculated using *t*-tests (Microsoft Excel, *t*-test, two-tailed distribution, unequal variance) using 2^RMA transformed values. Genes were considered significantly up-regulated/down-regulated if the *P*-value < 0.01 for all three iPSC-H1 comparisons. Using this statistical criterion, 350 probes were up-regulated and 238 probes were down-regulated in CSB-iPSC relative to H1. Differentially regulated genes were aggregated for gene ontology classification (DAVID v6.7, http://david.abcc.ncifcrf.gov/) using probe set IDs and the HuGene-1_0-st-v1 background data set. *P*-values used for determining significance were the multi-comparison corrected Benjamini *P*-values. The raw data from the microarray experiment are deposited at GEO, access number GSE 36648.

MicroRNA analysis

Total RNA isolated for two CSB-iPSC lines, five WT iPSC lines and two ES lines were treated as described in Illumina's Small RNA DIgital Gene Expression v1.5 with minor modifications to allow for sample indexing and multiplexing. Briefly, 1.5 μg Trizol (Invitrogen) extracted total RNA was ligated with a 3′ pre-adenylated adaptor using T4 RNA ligase 2, truncated (NEB), followed by ligation of a 5′ adaptor containing one of two 3′ barcoded indexes (ATCT, ACAC) using T4 RNA ligase 1 (NEB). First-strand cDNA synthesis was performed using Superscript II (Life Technologies) and DNA amplified using 12 cycles of PCR with Phusion polymerase (Finnzymes). Ninety to 115 bp DNA products were purified using a 8% non-denaturing acrylamide gel, eluted by diffusion, filtered using a Spin-X column (Costar) and precipitated. DNA was quantified using Quant-It PicoGreen (Life Technologies). Barcoded libraries were mixed and 17.5 fmol DNA per flowcell lane was sequenced on the Illumina GA2 for 36 cycles. Barcoded with ATCT were CSB-iPSC clone 1, WT-iPSC1, WT-iPSC2, WT-iPSC3 and huES3. Barcoded with ACAC were CSB-iPSC clone 3, WT-iPSC4, WT-iPSC5 and H1. Small RNA reads were mapped to the human (hg18) genome, and aligned with coordinates of known microRNAs from mirBase16. We required exact 5′ end alignment to the canonical microRNA, and identified isomiRs starting plus or minus one nucleotide from the canonical sequence. IsomiRs with a minimum read count of 50 reads per million reads, and consistently differentially expressed between CSB-to-WT samples were termed mis-regulated in the CSB-iPSCs (Supplementary Material, Table S1). Using seed sequence predictions from TargetScan v5.1, we correlated mis-regulated isomiRs and mRNA expression.

Immunostaining

Cells were fixed with 4% paraformaldehyde, followed by permeabilization and blocking with 0.1% (v/v) Triton X in PBS containing 5% (v/v) donkey serum, for 1 h. Primary antibodies were incubated overnight at 4°C. Samples were washed three times before secondary antibody incubation (Jackson Laboratories and Alexa Fluor Dyes, Life Technologies) for 1 h. Primary antibody concentrations were: α-Nanog mouse monoclonal 1:100 (BD Bioscience); α-Oct3/4 mouse monoclonal 1:250 (Santa Cruz); α-Lin28 goat polyclonal 1:400 (R&D Systems), α-Sox2 rabbit 1:400 (Chemicon) and α-SSEA-4 mouse monoclonal 1:200 (Millipore). Images were taken using a Zeiss inverted fluorescence microscope and processed with Adobe Photoshop CS4.

Embryoid body (EB) formation

iPSC colonies were kept for 2 days with hESC media supplemented with 10 ng/ml FGF-2. Cells were detached from matrigel-coated plates using dispase (0.5 mg/ml) and then plated in low-attachment dishes (Corning). EBs were kept under these conditions for ~10 days.

Teratoma formation in nude mice

Around $1-3 \times 10^6$ iPSCs were injected subcutaneously into the dorsal flanks of nude mice (CByJ.Cg-Foxn1nu/J) anesthetized with isoflurane. Six to 8 weeks after injection, teratomas were removed. Control mice injected with fibroblasts failed to form teratomas. All animal work was conducted according to the relevant national and international guidelines. Protocols were approved by the University of California San Diego Institutional Animal Care and Use Committee.

Electroporation and CSB knockdown

Human H9 ES cells were transfected with plasmids encoding shRNA against CSB (hairpin sequence 5′-CCGGC GTGGTTCAAATTACAGGTTTCTCGAGAAACCTGTAAT TTGAACCACGTTTTT-3′, pLKO.1-puro plasmid from Sigma-Aldrich) or a non-specific sequence (scrambled) as a control (as described in 49) by nucleofection (Amaxa Biosystems). Briefly, 1×10^6 H9 cells and 5 μg vector were resuspended in 5 μl nucleofactor solution and used for the nucleofection according to the manufacturer's instructions. After 48 h, the cell death ratio of shRNA-CSB and shRNA-Scrambled H9 transfected cells was determined by flow cytometry.

Flow cytometry experiments

Cells were fixed using cold 70% ethanol and kept at least 2 h at -20°C. Cells were washed with PBS and resuspended with 20 µg/ml Propidium Iodide (Sigma), 200 µl RNAse A (Life Technologies) and 0.2% Triton X-100 in PBS. All samples were incubated overnight at 4°C and DNA content was measured using FACsCalibur (BD).

ROS detection

Cells were seeded on matrigel-coated permanox chambers and after 3 days they were incubated with 25 µM carboxy-H_2DCFDA (Molecular Probes) for 30 min at 37°C, protected from light. Cells were gently washed with HBSS/Ca/Mg buffer and images were taken immediately using an inverted fluorescence microscope (Zeiss). TBHP (tert-butyl hydroperoxide 100 µM) treatment was used as a positive control. The quantification of the ROS production was addressed in two ways: (i) counting the number of fluorescent cells and (ii) measuring the intensity of the fluorescence emitted by the cells. The relative fluorescence intensity (arbitrary units ranging from 0 to 255, or black to white) was measured in randomly selected fields for each treatment and was analyzed and quantified using ImageProPlus software.

Maintenance of CSB-iPSCs under hypoxia

Cells were kept in the mTeSR media and 150 µM cobalt chloride (Sigma) was added for 24 h. After that, total protein was extracted using lysis buffer for the detection of HIF-1α levels by western blot. Replicates were fixed in cold 70% ethanol to perform cell death analysis in flow cytometry as described before.

SUPPLEMENTARY MATERIAL

Supplementary Material is available at *HMG* online.

ACKNOWLEDGEMENTS

FUNDING

REFERENCES

1. Weidenheim, K.M., Dickson, D.W. and Rapin, I. (2009) Neuropathology of Cockayne syndrome: evidence for impaired development, premature aging, and neurodegeneration. *Mech. Ageing Dev.*, **130**, 619–636.
2. Laugel, V., Dalloz, C., Durand, M., Sauvanaud, F., Kristensen, U., Vincent, M.C., Pasquier, L., Odent, S., Cormier-Daire, V., Gener, B. *et al.* (2010) Molecular analysis of mutations in the CSB (ERCC6) gene in patients with Cockayne syndrome. Mutation update for the CSB/ERCC6 and CSA/ERCC8 genes involved in Cockayne syndrome. *Hum. Mutat.*, **31**, 113–126.
3. Citterio, E., Van Den Boom, V., Schnitzler, G., Kanaar, R., Bonte, E., Kingston, R.E., Hoeijmakers, J.H. and Vermeulen, W. (2000) ATP-dependent chromatin remodeling by the Cockayne syndrome B DNA repair-transcription-coupling factor. *Mol. Cell Biol*, **20**, 7643–7653.
4. Newman, J.C., Bailey, A.D. and Weiner, A.M. (2006) Cockayne syndrome group B protein (CSB) plays a general role in chromatin maintenance and remodeling. *Proc. Natl Acad. Sci. USA*, **103**, 9613–9618.
5. Licht, C.L., Stevnsner, T. and Bohr, V.A. (2003) Cockayne syndrome group B cellular and biochemical functions. *Am. J. Hum. Genet.*, **73**, 1217–1239.
6. Yuan, X., Feng, W., Imhof, A., Grummt, I. and Zhou, Y. (2007) Activation of RNA polymerase I transcription by cockayne syndrome group B protein and histone methyltransferase G9a. *Mol. Cell*, **27**, 585–595.
7. Kyng, K.J., May, A., Brosh, R.M. Jr, Cheng, W.H., Chen, C., Becker, K.G. and Bohr, V.A. (2003) The transcriptional response after oxidative stress is defective in Cockayne syndrome group B cells. *Oncogene*, **22**, 1135–1149.
8. Filippi, S., Latini, P., Frontini, M., Palitti, F., Egly, J.M. and Proietti-De-Santis, L. (2008) CSB protein is (a direct target of HIF-1 and) a critical mediator of the hypoxic response. *EMBO J.*, **27**, 2545–2556.
9. Fousteri, M. and Mullenders, L.H. (2008) Transcription-coupled nucleotide excision repair in mammalian cells: molecular mechanisms and biological effects. *Cell Res.*, **18**, 73–84.
10. Dianov, G., Bischoff, C., Sunesen, M. and Bohr, V.A. (1999) Repair of 8-oxoguanine in DNA is deficient in Cockayne syndrome group B cells. *Nucleic Acids Res.*, **27**, 1365–1368.
11. Stevnsner, T., Nyaga, S., de Souza-Pinto, N.C., van der Horst, G.T., Gorgels, T.G., Hogue, B.A., Thorslund, T. and Bohr, V.A. (2002) Mitochondrial repair of 8-oxoguanine is deficient in Cockayne syndrome group B. *Oncogene*, **21**, 8675–8682.
12. Kyng, K.J. and Bohr, V.A. (2005) Gene expression and DNA repair in progeroid syndromes and human aging. *Ageing Res. Rev.*, **4**, 579–602.
13. Garinis, G.A., Uittenboogaard, L.M., Stachelscheid, H., Fousteri, M., van Ijcken, W., Breit, T.M., van Steeg, H., Mullenders, L.H., van der Horst, G.T., Brüning, J.C. *et al.* (2009) Persistent transcription-blocking DNA lesions trigger somatic growth attenuation associated with longevity. *Nat. Cell Biol.*, **11**, 604–615.
14. Liu, G.H., Barkho, B.Z., Ruiz, S., Diep, D., Qu, J., Yang, S.L., Panopoulos, A.D., Suzuki, K., Kurian, L., Walsh, C. *et al.* (2011) Recapitulation of premature ageing with iPSCs from Hutchinson-Gilford progeria syndrome. *Nature*, **472**, 221–225.
15. Zhang, J., Lian, Q., Zhu, G., Zhou, F., Sui, L., Tan, C., Mutalif, R.A., Navasankari, R., Zhang, Y., Tse, H.F. *et al.* (2011) A human iPSC model of Hutchinson Gilford Progeia reveals vascular smooth muscle and mesenchymal stem cell defects. *Cell Stem Cell*, **8**, 31–45.
16. Colella, S., Nardo, T., Botta, E., Lehmann, A.R. and Stefanini, M. (2000) Identical mutations in the CSB gene associated with either Cockayne syndrome or the DeSanctis-cacchione variant of xeroderma pigmentosum. *Hum. Mol. Genet.*, **9**, 1171–1175.
17. Takahashi, K., Tanabe, K., Ohnuki, M., Narita, M., Ichisaka, T., Tomoda, K. and Yamanaka, S. (2007) Induction of pluripotent stem cells from adult human fibroblasts by defined factors. *Cell*, **131**, 861–872.
18. Yoshida, K. and Miki, Y. (2010) The cell death machinery governed by the p53 tumor suppressor in response to DNA damage. *Cancer Sci.*, **101**, 831–835.
19. Marmorstein, L.Y., Ouchi, T. and Aaronson, S.A. (1998) The BRCA2 gene product functionally interacts with p53 and RAD51. *Proc. Natl Acad. Sci. USA*, **95**, 13869–13874.
20. Nishiyama, A., Matsui, M., Iwata, S., Hirota, K., Masutani, H., Nakamura, H., Takagi, Y., Sono, H., Gon, Y. and Yodoi, J. (1999) Identification of

thioredoxin-binding protein-2/vitaminD(3) up-regulated protein 1 as a
negative regulator of thioredoxin function and expression. *J. Biol. Chem.*,
274, 21645–21650.
21. Yoshihara, E., Chen, Z., Matsuo, Y., Masutani, H. and Yodoi, J. (2010)
Thiol redox transitions by thioredoxin and thioredoxin-binding protein-2
in cell signaling. *Methods Enzymol.*, **474**, 67–82.
22. Griffiths-Jones, S. (2004) The microRNA Registry. *Nucleic Acid Res.*, **32**,
D109–D11.
23. Griffiths-Jones, S., Grocock, R.J., van Dongen, S., Bateman, A. and
Enright, A.J. (2006) miRBase: microRNA sequences, targets and gene
nomenclature. *Nucleic Acid Res.*, **34**, D140–D144.
24. Griffiths-Jones, S., Saini, H.K., van Dongen, S. and Enright, A.J. (2008)
miRBase: tools for microRNA genomics. *Nucleic Acid Res.*, **36**,
D154–D158.
25. Kozomara, A. and Griffiths-Jones, S. (2011) miRBase: integrating
microRNA annotation and deep-sequencing data. *Nucleic Acid Res.*, **39**,
D152–D157.
26. Lee, L.W., Zhang, S., Etheridge, A., Ma, L., Martin, D., Galas, D. and
Wang, K. (2010) Complexity of the microRNA repertoire revealed by
next-generation sequencing. *RNA*, **16**, 2170–2180.
27. Burroughs, A.M., Ando, Y., de Hoon, M.J., Tomaru, Y., Suzuki, H.,
Hayashizaki, Y. and Daub, C.O. (2011) Deep-sequencing of human
Argonaute-associated small RNAs provides insight into miRNA sorting
and reveals Argonaute association with RNA fragments of diverse origin.
RNA Biol., **8**, 158–177.
28. Lewis, B.P., Burge, C.B. and Bartel, D.P. (2005) Conserved seed pairing,
often flanked by adenosines, indicates that thousands of human genes are
microRNA targets. *Cell*, **120**, 15–20.
29. Liu, M., Wang, Z., Yang, S., Zhang, W., He, S., Hu, C., Zhu, H., Quan, L.,
Bai, J. and Xu, N. (2011) TNF-α is a novel target of miR-19a.
Int. J. Oncol., **38**, 1013–1022.
30. Circu, M.L. and Aw, T.Y. (2010) Reactive oxygen species, cellular redox
systems, and apoptosis. *Free Radic. Biol. Med.*, **48**, 749–762.
31. Mammucari, C. and Rizzuto, R. (2010) Signaling pathways in
mitochondrial dysfunction and aging. *Mech. Ageing Dev.*, **131**, 536–543.
32. Pandita, T.K. and Richardson, C. (2009) Chromatin remodeling finds its
place in the DNA double-strand break response. *Nucleic Acids Res.*, **7**,
1363–1377.
33. Brusevold, I.J., Husvik, C., Schreurs, O., Schenck, K., Bryne, M. and
Søland, T.M. (2010) Induction of invasion in an organotypic oral cancer
model by CoCl2, a hypoxia mimetic. *Eur. J. Oral Sci.*, **118**, 168–176.
34. Ema, M., Hirota, K., Mimura, J., Abe, H., Yodoi, J., Sogawa, K.,
Poellinger, L. and Fujii-Kuriyama, Y. (1999) Molecular mechanisms of
transcription activation by HLF and HIF1alpha in response to hypoxia:
their stabilization and redox signal-induced interaction with CBP/p300.
EMBO J., **18**, 1905–1914.
35. Takahashi, K. and Yamanaka, S. (2006) Induction of pluripotent stem
cells from mouse embryonic and adult fibroblast cultures by defined
factors. *Cell*, **126**, 663–676.
36. Liu, H., Zhu, F., Yong, J., Zhang, P., Hou, P., Li, H., Jiang, W., Cai, J.,
Liu, M., Cui, K. *et al.* (2008) Generation of induced pluripotent stem cells
from adult rhesus monkey fibroblasts. *Cell Stem Cell*, **3**, 587–590.
37. Ezashi, T., Telugu, B.P., Alexenko, A.P., Sachdev, S., Sinha, S. and
Roberts, R.M. (2009) Derivation of induced pluripotent stem cells from
pig somatic cells. *Proc. Natl Acad. Sci. USA*, **106**, 10993–10998.
38. Banito, A., Rashid, S.T., Acosta, J.C., Li, S., Pereira, C.F., Geti, I., Pinho,
S., Silva, J.C., Azuara, V., Walsh, M. *et al.* (2009) Senescence impairs
successful reprogramming to pluripotent stem cells. *Genes Dev.*, **23**,
2134–2139.
39. Marión, R.M., Strati, K., Li, H., Murga, M., Blanco, R., Ortega, S.,
Fernandez-Capetillo, O., Serrano, M. and Blasco, M.A. (2009) A
p53-mediated DNA damage response limits reprogramming to ensure iPS
cell genomic integrity. *Nature*, **460**, 1149–1153.
40. Hong, H., Takahashi, K., Ichisaka, T., Aoi, T., Kanagawa, O., Nakagawa,
M., Okita, K. and Yamanaka, S. (2009) Suppression of induced
pluripotent stem cell generation by the p53-p21 pathway. *Nature*, **460**,
1132–1135.
41. Li, H., Collado, M., Villasante, A., Strati, K., Ortega, S., Cañamero, M.,
Blasco, M.A. and Serrano, M. (2009) The Ink4/Arf locus is a barrier for
iPS cell reprogramming. *Nature*, **460**, 1136–1139.
42. Utikal, J., Polo, J.M., Stadtfeld, M., Maherali, N., Kulalert, W., Walsh,
R.M., Khalil, A., Rheinwald, J.G. and Hochedlinger, K. (2009)
Immortalization eliminates a roadblock during cellular reprogramming
into iPS cells. *Nature*, **460**, 1145–1148.
43. Raya, A., Rodríguez-Pizà, I., Guenechea, G., Vassena, R., Navarro, S.,
Barrero, M.J., Consiglio, A., Castellà, M., Río, P., Sleep, E. *et al.* (2009)
Disease-corrected haematopoietic progenitors from Fanconi anaemia
induced pluripotent stem cells. *Nature*, **460**, 53–59.
44. Fong, Y.W., Inouye, C., Yamaguchi, T., Cattoglio, C., Grubisic, I. and
Tjian, R. (2011) A DNA repair complex functions as an Oct4/Sox2
coactivator in embryonic stem cells. *Cell*, **147**, 120–131.
45. Wang, Y., De Keulenaer, G.W. and Lee, R.T. (2002) Vitamin
D(3)-up-regulated protein-1 is a stress-responsive gene that regulates
cardiomyocyte viability through interaction with thioredoxin. *J. Biol.
Chem.*, **277**, 26496–26500.
46. Han, S.H., Jeon, J.H., Ju, H.R., Jung, U., Kim, K.Y., Yoo, H.S., Lee, Y.H.,
Song, K.S., Hwang, H.M., Na, Y.S. *et al.* (2003) VDUP1 upregulated by
TGF-beta1 and 1,25-dihydorxyvitamin D3 inhibits tumor cell growth by
blocking cell-cycle progression. *Oncogene*, **22**, 4035–4046.
47. Yoshida, T., Nakamura, H., Masutani, H. and Yodoi, J. (2005) The
involvement of thioredoxin and thioredoxin binding protein-2 on cellular
proliferation and aging process. *Ann. N. Y. Acad. Sci.*, **1055**, 1–12.
48. Frontini, M. and Proietti-De-Santis, L. (2009) Cockayne syndrome B
protein (CSB): linking p53, HIF-1 and p300 to robustness, lifespan, cancer
and cell fate decisions. *Cell Cycle*, **8**, 693–696.
49. Marchetto, M.C., Carromeu, C., Acab, A., Yu, D., Yeo, G.W., Mu, Y.,
Chen, G., Gage, F.H. and Muotri, A.R. (2010) A model for neural
development and treatment of Rett syndrome using human induced
pluripotent stem cells. *Cell*, **43**, 527–539.